

A verification of the gyrokinetic microstability codes GEM, GYRO, and GS2

R. V. Bravenec,^{1,a)} Y. Chen,² J. Candy,³ W. Wan,² and S. Parker²

¹*Fourth State Research, 503 Lockhart Dr., Austin, Texas 78704-4335, USA*

²*University of Colorado, Boulder, Colorado 80309, USA*

³*General Atomics, P.O. Box 85608, San Diego, California 92186-5608, USA*

(Received 8 August 2013; accepted 9 October 2013; published online 25 October 2013)

A previous publication [R. V. Bravenec *et al.*, Phys. Plasmas **18**, 122505 (2011)] presented favorable comparisons of linear frequencies and nonlinear fluxes from the Eulerian gyrokinetic codes GYRO [J. Candy and R. E. Waltz, J. Comput. Phys. **186**, 545 (2003)] and gs2 [W. Dorland *et al.*, Phys. Rev. Lett. **85**, 5579 (2000)]. The motivation was to verify the codes, i.e., demonstrate that they correctly solve the gyrokinetic-Maxwell equations. The premise was that it is highly unlikely for both codes to yield the same incorrect results. In this work, we add the Lagrangian particle-in-cell code GEM [Y. Chen and S. Parker, J. Comput. Phys. **220**, 839 (2007)] to the comparisons, not simply to add another code, but also to demonstrate that the codes' algorithms do not matter. We find good agreement of GEM with GYRO and gs2 for the plasma conditions considered earlier, thus establishing confidence that the codes are verified and that ongoing validation efforts for these plasma parameters are warranted. © 2013 AIP Publishing LLC. [<http://dx.doi.org/10.1063/1.4826511>]

The physics capabilities of today's gyrokinetic microstability codes are so extensive that they cannot be fully verified for actual tokamak plasmas using purely analytic approaches. Instead, verification—"the process by which it is determined that a numerical algorithm correctly solves a mathematical model [here, gyrokinetic-Maxwell] within a set of specified, predetermined tolerances"¹—must rely on comparing code results for identical plasmas and physics (benchmarking). The assumption is that it is highly unlikely for all codes to yield the same erroneous results.

In a previous paper,² linear and nonlinear simulations by the codes GYRO³ and gs2 (Ref. 4) were compared for the plasma parameters of a low-power L-mode DIII-D discharge at $\rho = 0.5$, where ρ is the square root of the normalized toroidal flux. The benchmarks included plasma shaping, kinetic electrons, collisions, one impurity, and electromagnetic effects—referred to as "full physics." The complex linear frequencies agreed closely, as did the time-averaged nonlinear fluxes within the uncertainties due to their natural time variation. That work compared two codes using the same algorithm (Eulerian grid). Here, we add to the comparisons the particle-in-cell (PIC) code GEM⁵ that employs a Lagrangian grid. Not only would three-code agreement be a more convincing verification exercise, but it also would establish that the commonality of GYRO's and gs2's algorithm is not the sole source of their agreement.

The previous verification studies were carried out in the flux-tube geometry.⁶ GEM, on the other hand, is a global code. In order to facilitate a direct comparison with GYRO and gs2, it was necessary to implement a flux-tube model in GEM. Further details may be found in Ref. 7. The time step, spatial grids, simulation box size, and number of particles were sufficient to achieve near invariance of the GEM results with

small variations of these parameters, as was the case with GYRO and gs2. (Of course, it is impractical to perform these "convergence" tests to an arbitrarily exact degree.) Descriptions of GYRO and gs2, details of the computations, and the verification procedure can be found in Ref. 2. Both GEM and gs2 are run as initial-value solvers, as is GYRO unless otherwise noted.

We again analyze the DIII-D discharge 128913 at 1.5 s into the discharge at the radius $\rho = 0.5$ ($r/a \approx 0.55$, where r is the half-width of the flux surface at the elevation of the centroid and a is the value of r at the outermost flux surface.⁸) Local plasma parameters are listed in Table I of Ref. 2 and defined therein.

The normalized real and imaginary linear frequencies (hereafter referred to as "frequencies" and "growth rates," respectively) versus normalized poloidal wave number $k_{\theta}\rho_s$ are shown in Fig. 1 for full physics. The content of the figure is identical to that of Fig. 1 of Ref. 2 except for the additional GEM results. They are not shown for $k_{\theta}\rho_s \geq 2$ because GEM averages over the ion orbits at only four points (increasing the number is not trivial), so it loses accuracy with increasing wave number. Therefore, we restrict attention to $k_{\theta}\rho_s \leq 2$ in the remainder of this work. This allows the assumption of drift-kinetic electrons here and in the collisionless case following. The omission of comparisons among codes at higher wave numbers does not impact comparisons of the nonlinear fluxes, as will be explained later.

The real frequencies from GEM agree closely with those from GYRO and gs2. In the region of $k_{\theta}\rho_s \approx 1.2$, ion-temperature-gradient (ITG) modes transition to trapped-electron modes (TEMs). At the transition, it becomes problematic to accurately extract a single frequency from the initial-value computations because both modes have the same small growth rate. This occurs at $k_{\theta}\rho_s \approx 1.15$ (red/blue dashed line) for GYRO and gs2, but at $k_{\theta}\rho_s \approx 1.25$ (green dotted line) for GEM. The growth rates from GEM agree with those from

^{a)}Author to whom correspondence should be addressed. Electronic mail: rvbravenec@4th-state.com

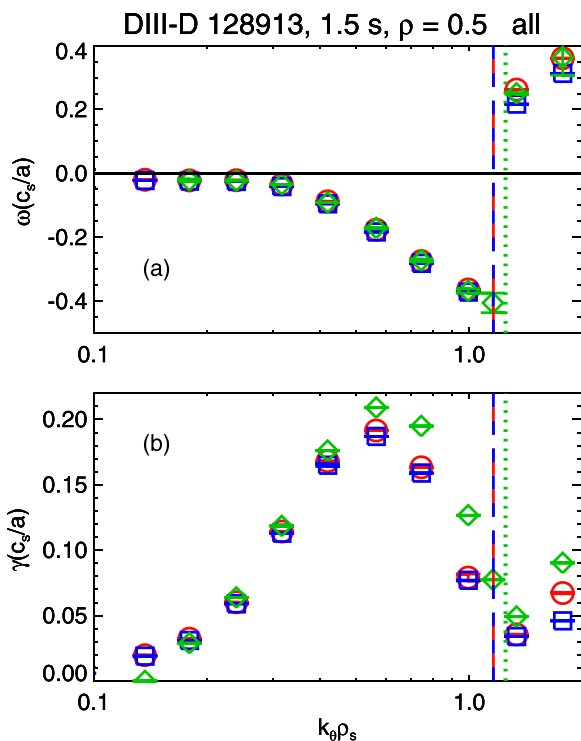


FIG. 1. Normalized (a) real frequencies and (b) growth rates versus normalized wave numbers $0.1 \leq k_{\theta}\rho_s \leq 2.0$ for full-physics from GYRO (red circles), GS2 (blue squares), and GEM (green diamonds). Vertical dashed lines indicate approximate wave numbers where the computations fail to converge to a single mode: GYRO in red (—), GS2 in blue (- - -), and GEM in green (.....). The omission of a real frequency from GEM at the lowest wave number is because the mode is stable.

GYRO and GS2 at the lower wave numbers but diverge toward higher wave numbers. The precise cause(s) of the differences between GEM and the Eulerian codes near the transition region is not well understood. However, experience shows that often minor differences in resolution and/or algorithm can have significant effects in the vicinity of a mode transition (for example, see Fig. 1 of Ref. 9).

In the spirit of identifying the source(s) of differences among codes, we remove physics components one at a time searching for agreement. As in Ref. 2, we first remove collisions. Fig. 2 shows the addition of GEM results to the collisionless case in Fig. 2 of Ref. 2. There is not only good agreement of the real frequencies between GEM and GYRO/GS2, but there is also better agreement in the growth rates compared to the collisional results. To better characterize the transition region, we have added results from GYRO eigenmode analysis (continuous curves).⁹ (Eigenmode results were not presented in Fig. 1 because of subtle differences in the collision operator.) Except for GEM at $k_{\theta}\rho_s = 0.57$, we note excellent agreement among all the codes between the dominant eigenmodes (largest growth rates) and the initial-value results. The eigenmode analysis shows the ITG-TEM hybrid modes at low wave numbers transition to a pure TEM branch at $k_{\theta}\rho_s \approx 0.65$ (vertical red dashed line), where the growth rates are equal. The ITG branch continues to higher wave numbers but is subdominant and stabilizes at $k_{\theta}\rho_s \approx 1.15$. The initial-value calculations of all the codes transition to the TEM at essentially the same wave number. The improved agreement between GEM and the

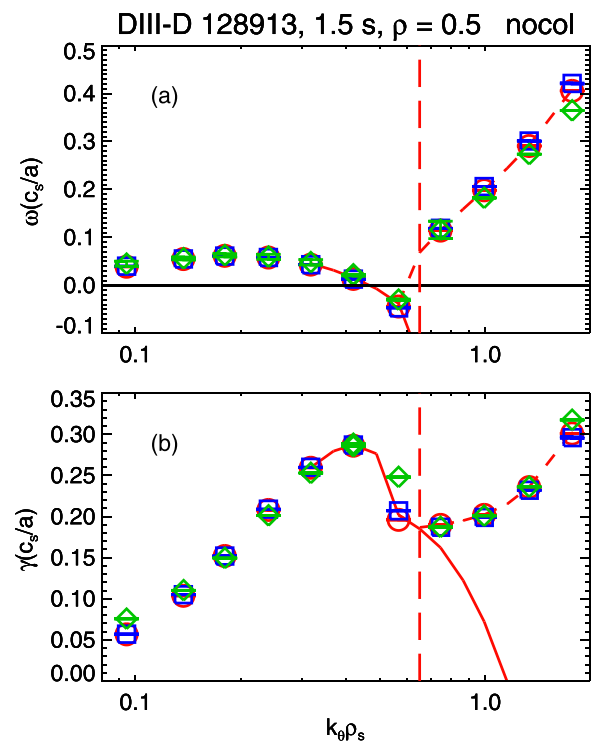


FIG. 2. Same as Fig. 1 except ignoring collisions. Also shown are results from GYRO eigenmode analysis, where the ITG and TEM branches are indicated by the solid and dashed red curves, respectively. The wave number where the growth rates are equal is indicated by the vertical red dashed line. The GEM real frequencies below $k_{\theta}\rho_s = 0.5$ are within $\pm 0.01 c_s/a$ of those of GYRO and GS2.

Eulerian codes without collisions suggests differences in the effects of essentially identical collision operators that manifest themselves in the approach to and in the TEM regime. This further suggests that the differences between GEM and GYRO/GS2 are due to algorithm, perhaps involving velocity-space resolution. This is a topic of further study.

Although not shown here, GEM computations for adiabatic electrons agree well with those from GYRO and GS2 shown in Fig. 3 of Ref. 2. Linear comparison among codes also has been performed without collisions or impurities.⁷ The computations were performed not only for the shaped plasma—with both kinetic and adiabatic electrons—but also for a circular cross-section. Agreement among codes is excellent for these reduced-physics cases. This demonstrates that agreement at the higher levels of physics realism presented here is not due to a chance cancellation of errors at lower levels.

We next turn to nonlinear simulations. The velocity space resolution in a PIC code is determined by the number of particles per spatial cell, a typical value being 32. Like in GYRO and GS2, the toroidal mode numbers retained in GEM are multiples of the mode number having a wavelength equal to the simulation box dimension L_y , where y is the bi-normal direction in the field-aligned coordinate. Filtering in Fourier space can be performed prior to the inverse transform into real space, so that poorly resolved modes can be removed. The highest resolved wave number is determined by the number of grid points in y , which here is 32, giving $(k_{\theta}\rho_s)_{\max} \approx 2$. As for the GYRO and GS2 simulations, we impose a

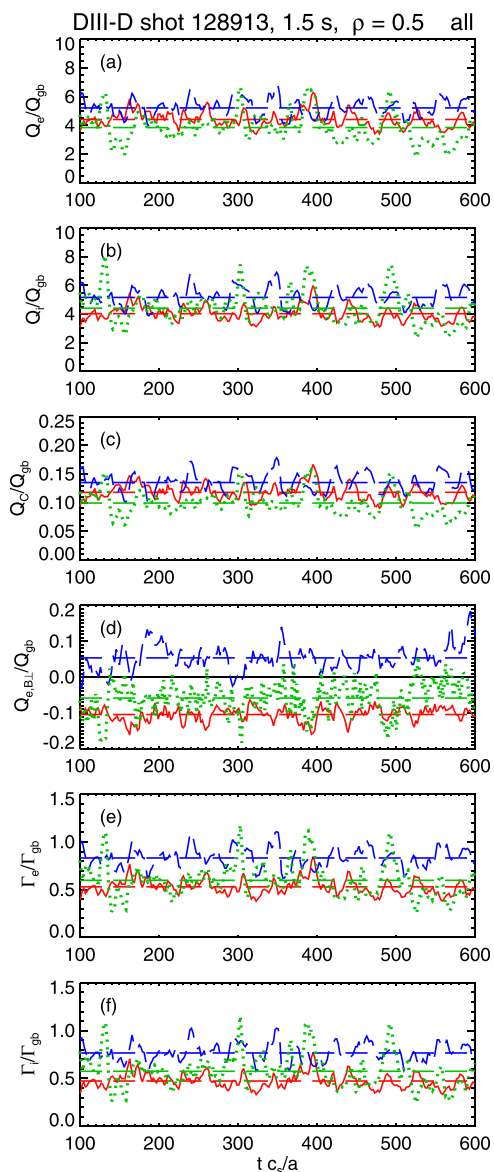


FIG. 3. Gyro-Bohm-normalized (a) electron, (b) main ion (D), (c) and impurity ion (C^{6+}) electrostatic energy fluxes, (d) electron energy flux from \mathbf{B}_\perp fluctuations, and (e) electron and (f) main ion electrostatic particle fluxes including collisions (corresponds to linear results of Fig. 1). GYRO in red (—), gs2 in blue (---), and GEM in green (.....). Time is normalized to the sound transit time a/c_s . Straight dashed lines indicate averages over the time range shown.

cut-off at $k_\theta \rho_s \approx 1$ even if modes with higher wave numbers are well resolved. As shown in Ref. 2, this cutoff is justified because the GYRO and gs2 flux spectra decay to less than 10% of their peaks by $k_\theta \rho_s = 1$. (This result minimizes the significance of the GEM upper wave-number limit of $k_\theta \rho_s \approx 2$.) Information about temporal, spatial, and velocity-space resolutions, simulation box size, etc. for the GYRO and gs2 simulations are found in Ref. 2.

Fluxes are normalized to the gyro-Bohm fluxes defined in Ref. 2. To gauge agreement between any two codes, we utilize the metric Δ , also defined in Ref. 2. For a given flux, the metric is zero for perfect agreement between the time averages and unity if the average of either flux lies within a standard deviation of the other. As in Ref. 2, we define agreement between codes 1 and 2 as $\Delta_{12} < 1$.

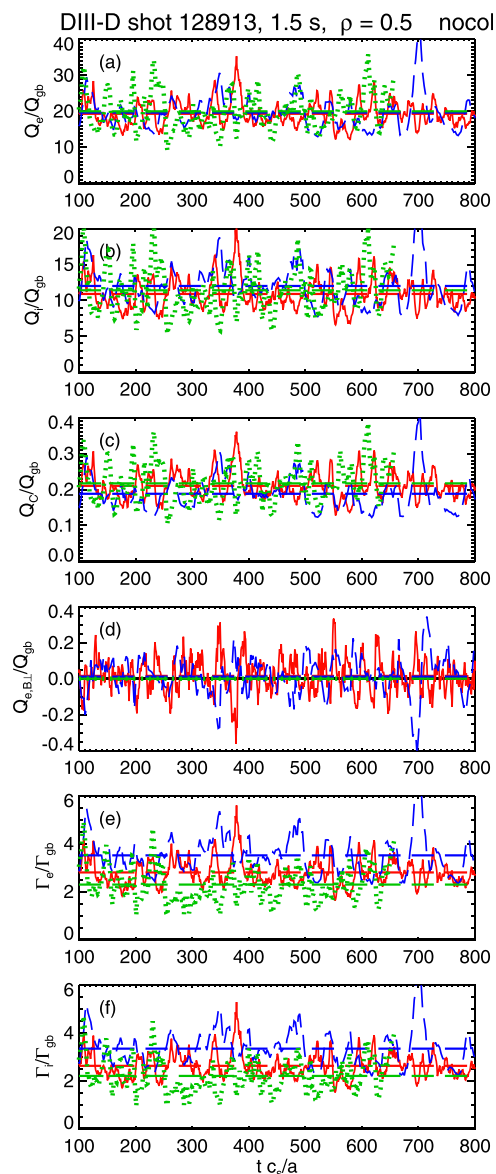


FIG. 4. Same as Fig. 3 except omitting collisions. (Average GEM fluxes are computed over 100 to 650 a/c_s and the fluxes are the sum of electrostatic and electromagnetic fluxes.)

Shown in Fig. 3 (with collisions) and Fig. 4 (collisionless) are time traces of the normalized (a) electron, (b) main ion, and (c) impurity ion (C^{6+}) electrostatic energy fluxes, (d) electron energy flux from \mathbf{B}_\perp fluctuations, and (e) electron and (f) main ion electrostatic particle fluxes. (By charge conservation, the impurity particle flux Γ_C is simply $(\Gamma_e - \Gamma_i)/6$, so it is not shown.) The time averages with standard deviations and the agreement metrics are found in Tables I and II. The values of the GYRO and gs2 average fluxes and the metrics are taken from Ref. 2. Likewise, comparisons between GYRO and gs2 are discussed there, so we address only GEM/GYRO and GEM/GS2 comparisons here.

From Table I, we see that GEM agrees better (by the criterion $\Delta < 1$) with GYRO and gs2 (except for the small carbon energy flux) than the latter agree with each other. However, in the case of the electron energy flux, this is simply a consequence of the larger time variation of the fluxes from GEM. The fact that the GEM fluxes agree as well as they do with gs2

TABLE I. Normalized fluxes and measures of agreement among codes for simulations with collisions.

	GYRO	GS2	GEM	$\Delta_{\text{GYRO/GS2}}$	$\Delta_{\text{GEM/GYRO}}$	$\Delta_{\text{GEM/GS2}}$
Q_e/Q_{gB}	4.41 ± 0.54	5.24 ± 0.60	4.00 ± 0.96	1.37	0.44	1.28
Q_i/Q_{gB}	4.03 ± 0.52	5.18 ± 0.64	4.54 ± 1.06	1.80	0.49	0.58
Q_C/Q_{gB}	0.118 ± 0.014	0.136 ± 0.016	0.10 ± 0.02	1.08	0.80	1.64
$Q_{B\perp}/Q_{gB}$	-0.104 ± 0.019	0.054 ± 0.0366	-0.06 ± 0.04	4.32	0.96	2.64
Γ_e/Γ_{gB}	0.530 ± 0.080	0.835 ± 0.102	0.62 ± 0.17	2.98	0.49	1.25
Γ_i/Γ_{gB}	0.473 ± 0.075	0.770 ± 0.097	0.59 ± 0.17	3.07	0.70	1.02

TABLE II. Normalized fluxes and measures of agreement among codes for simulations without collisions.

	GYRO	GS2	GEM	$\Delta_{\text{GYRO/GS2}}$	$\Delta_{\text{GEM/GYRO}}$	$\Delta_{\text{GEM/GS2}}$
Q_e/Q_{gB}	19.3 ± 3.4	19.7 ± 4.6	20.0 ± 5.2	0.08	0.13	0.07
Q_i/Q_{gB}	10.9 ± 2.1	12.0 ± 2.9	11.4 ± 3.2	0.39	0.16	0.19
Q_C/Q_{gB}	0.21 ± 0.04	0.19 ± 0.05	0.22 ± 0.05	0.47	0.13	0.54
$Q_{B\perp}/Q_{gB}$	0.015 ± 0.096	0.013 ± 0.106	...	0.024
Γ_e/Γ_{gB}	2.81 ± 0.55	3.53 ± 0.82	2.30 ± 0.73	0.88	0.69	1.49
Γ_i/Γ_{gB}	2.63 ± 0.51	3.36 ± 0.78	2.21 ± 0.71	0.93	0.60	1.46

and GYRO (in particular, GYRO) indicates that the divergence of the growth rates approaching the TEM region shown in Fig. 1 does not greatly impact the fluxes. This, in turn, is consistent with the flux spectra shown in Fig. 5 of Ref. 2, which peaks well below the transition region.

As in Ref. 2, we next omit collisions to examine if any differences in their implementation in GEM may be responsible for the small differences with GYRO and GS2. The fluxes are shown in Fig. 4 and the averages and metrics are given in Table II. (The GEM simulation was performed with an earlier version of the code that computed the sum of the electrostatic and electromagnetic fluxes. These are plotted as electrostatic because a subsequent shorter simulation with separate components indicated that the electromagnetic fluxes were negligible, as are the GYRO and GS2 fluxes shown here.) We observe that all the fluxes agree well among codes except for the particle fluxes between GEM and GS2 (again, by the criterion $\Delta < 1$), but like the collisional particle fluxes, they are small compared to the electron and ion energy fluxes.

As seen in Ref. 2, the magnitudes of all but the electromagnetic flux are much greater without collisions. This can explain some of the poorer relative agreement among the codes when including collisions: the absolute differences among the average fluxes with collisions are of the same order as those without them. Thus, none of the fluxes exhibit large absolute differences among the codes.

We have shown that three codes with different algorithms (Eulerian and Lagrangian) yield essentially the same complex linear frequencies within the wave-number range relevant to the nonlinear fluxes and the fluxes themselves within uncertainties from the natural time variations. This provides evidence that the codes correctly solve the gyrokinetic-Maxwell equations and are therefore verified for

the plasma parameters employed here and in Ref. 2. Because these parameters are also utilized in validation exercises described in Refs. 10 and 11, the verification results presented here legitimize the validation work.

This work was supported by the U.S. Department of Energy under Grant Nos. DE-FG02-08ER54978, DE-FG02-08ER54954, DE-FG02-08ER54987, and DE-FG03-95ER54309. The simulations were performed on the Hopper system at the National Energy Research Scientific Computing Center that is supported by the Office of Science of the U.S. Department of Energy under Contract No. DE-AC02-05CH11231.

¹P. W. Terry, M. Greenwald, J.-N. Leboeuf, G. R. McKee, D. R. Mikkelsen, W. M. Nevins, D. E. Newman, and D. P. Stotler, "Task group on verification and validation, U.S. burning plasma organization, and U.S. transport task force," *Phys. Plasmas* **15**, 062503 (2008).

²R. V. Bravenec, J. Candy, M. Barnes, and C. Holland, *Phys. Plasmas* **18**, 122505 (2011).

³J. Candy and R. E. Waltz, *J. Comput. Phys.* **186**, 545 (2003).

⁴W. Dorland, F. Jenko, M. Kotschenreuther, and B. N. Rogers, *Phys. Rev. Lett.* **85**, 5579 (2000).

⁵Y. Chen and S. Parker, *J. Comput. Phys.* **220**, 839 (2007).

⁶M. A. Beer, S. C. Cowley, and G. W. Hammett, *Phys. Plasmas* **2**, 2687 (1995).

⁷Y. Chen, S. E. Parker, W. Wan, and R. Bravenec, *Phys. Plasmas* **20**, 092511 (2013).

⁸R. L. Miller, M. S. Chu, J. M. Greene, Y. R. Lin-Liu, and R. E. Waltz, *Phys. Plasmas* **5**, 973 (1998); R. E. Waltz and R. L. Miller, *ibid.* **6**, 4265 (1999); J. Candy, *Plasma Phys. Controlled Fusion* **51**, 105009 (2009).

⁹E. A. Belli and J. Candy, *Phys. Plasmas* **17**, 112314 (2010).

¹⁰C. Holland, A. E. White, G. R. McKee, M. W. Shafer, J. Candy, R. E. Waltz, L. Schmitz, and G. R. Tynan, *Phys. Plasmas* **16**, 052301 (2009).

¹¹A. E. White, W. A. Peebles, T. L. Rhodes, C. H. Holland, G. Wang, L. Schmitz, T. A. Carter, J. C. Hillesheim, E. J. Doyle, L. Zeng, G. R. McKee, G. M. Staebler, R. E. Waltz, J. C. DeBoo, C. C. Petty, and K. H. Burrell, *Phys. Plasmas* **17**, 056103 (2010).